A Novel Inkjet-Printed Chipless RFID-Based Passive Fluid Sensor Platform

Sangkil Kim†, James Cooper and Manos M. Tentzeris
School of Electrical and Computer Engineering
Georgia Institute of Technology
Atlanta, GA, USA
†ksangkil3@gatech.edu

Robert Herre
Lehrstuhl fül Technische Elektronik (LTE)
Friedrich-Alexander-Universität Erlangen-Nürnberg
Erlangen, Germany
robert@herre.biz

Sijia Gu† and Tuami Lasri
Institut d'Electronique
de Microélectronique et de Nanotechnologie (IEMN-DHS)
UMR CNRS 8520 - Université Lille 1, Villeneuve d'Ascq, France
†kusucar@gmail.com

***Abstract*—In this paper, we present a novel chipless RFID-based passive fluid sensor platform which enables a reliable remote fluid identification. The proposed sensor platform consists of a capacitive gap-loaded tunable filter for fluid sensing and two broadband perpendicularly polarized microstrip monopole antennas for a dual-polarization wireless interrogation approach, that allows for drastically reduced ambient clutter interference. Two different fluids (acetone and water) are tested to verify the exceptional sensing capability of the proposed platform, while inkjet-printing technology has been used for its low-cost conformal implementation.**

I. INTRODUCTION

RFID-based sensor is a very fast growing area with numerous advantages, especially in wireless sensing topologies [1-3]. These sensors feature a very simple structure that enables a low-cost implementation that is compatible with conventional wireless sensor networks (WSN) and RFID infrastructure [1]. Recently developed large-area fabrication processes, such as inkjet printing [2], can be easily utilized for the scalable production of RFID-based wireless sensors, while zero-power implementations can be realized utilizing chipless passive RFID approaches.

In this work, a novel fully passive zero-power RFID-based fluidic sensor platform, that utilizes a capacitive method for the detection of different fluids and a dual-polarization (horizontal/vertical) response for a clutter-interference-free remote interrogation, is introduced. The proposed sensor platform needs only a single drop (~ 50 μL) of a fluid sample for detection and requires zero-power since a chipless RFID-based sensor topology is utilized.

In section II, the design of the proposed passive RFID-based fluid sensor platform is presented, while in section III, an inkjet-printed prototype of the proposed sensor platform is discussed, followed by a conclusion.

This work is supported by National Science Foundation (NSF).

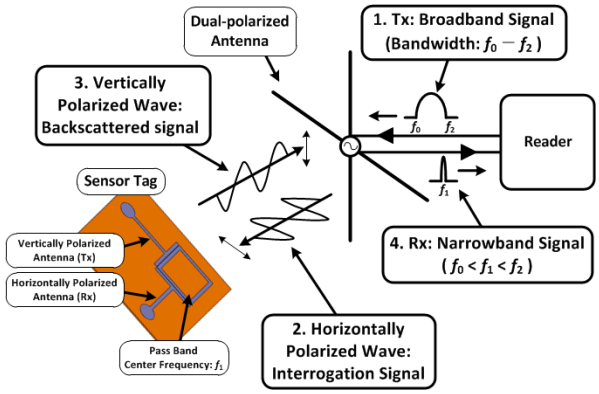

Fig. 1. Operation principle of the proposed chipless RFID-based sensor system

II. A CHIPLESS RFID-BASED SENSOR PLATFORM DESIGN

A. Operation Principle

The operation principle of the proposed RFID-based passive sensor system is depicted in Fig. 1. The frequency band of 2.2 GHz ~ 2.6 GHz has been chosen because it includes the ISM band around 2.4 GHz, whereas the proposed design can be easily scaled up to any other frequencies. Due to the liquid-dependent capacitance change of the loaded capacitive gap of a microstrip square-ring resonator filter, the center frequency of the filter's pass band shifts lower when a high-dielectric material, such as water, is loaded on the gap. Two orthogonally polarized broadband microstrip monopole antennas are integrated with the filter to enable wireless interrogation by exploiting the dual-polarization property. The horizontally polarized antenna (Rx antenna) receives a broadband pulse signal (bandwidth: $f_2 - f_0$) in frequency domain while the vertically polarized antenna (Tx antenna) reradiates a filtered broadband signal (narrowband signal at f_1), and vice versa. The reader also utilizes a broadband antenna

978-1-4673-4642-9/13/$31.00 ©2013 IEEE

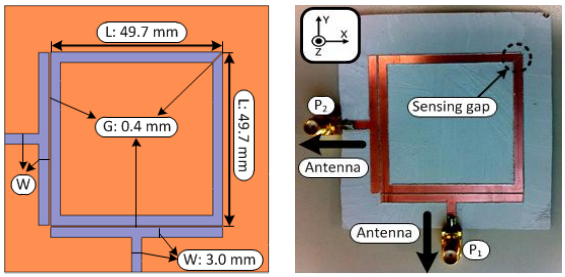

(a) (b)

Fig. 2. (a) Dimensions of the capacitive gap-loaded tunable ring resonator filter for capacitive sensing and (b) the fabricated prototype.

with the dual polarization to interrogate the dual polarized sensor platform. It interrogates the sensor platform with a broadband signal which has a bandwidth of $f_2 - f_0$, and receives the backscattered narrowband signal from the sensor platform at the frequency of f_1. The loaded material on the sensor platform can be detected by observing the shift of the center frequency of the backscattered narrowband signal that is strongly dependent on the relative dielectric constant (ε_r) of the loaded material on the filter's capacitive gap.

B. Capacitive Gap-loaded Tunable Filter

The capacitive gap-loaded microstrip square ring resonator is the main sensing component of the proposed passive sensor tag. A square-shaped ring resonator has been chosen to achieve a dual polarization property by placing two linearly polarized antennas in an orthogonal configuration, while it allows for an easy fabrication. The perimeter of the resonator has been chosen to be equal to one wavelength (λ_0) at the operation frequency of 2.6 GHz (center frequency for air-filled capacitive gap), and it should be optimized to resonate at desired operation frequency when the capacitive gap is introduced in the ring resonator. The capacitance introduced by the gap decreases the total capacitance of the ring resonator which results in shift of the resonant frequency to higher frequencies [4]. The chosen perimeter of the square-shaped ring resonator operating at 2.6 GHz is 198.8 mm which results in the edge length of 49.7 mm. The width (G) of the coupled feeding gap, that serves as the capacitive sensor, is the most critical design parameter because it determines the center frequency of the filter's pass band [5]. A narrower gap is better for low insertion loss (IL) because the coupling coefficient is inversely proportional to the width of the gap [6]. Furthermore, the width of the capacitive sensor gap significantly affects the sensitivity of the sensor. Narrower gaps result in larger variation range of the capacitance depending on the loaded material as the capacitance increases. Thus, it is desirable to make the gap as narrow as possible in this kind of application. The chosen width of the coupled feeding and the capacitive sensor gap is 0.4 mm because of the fabrication limitation. The width of the feeding line and the ring resonator is chosen to be equal to 3 mm to keep the impedance of the microstrip line to 50 Ω. Fig. 2 shows the geometry and the fabricated capacitive gap-loaded tunable filter. The filter is fabricated on RO3003 [7] which has a relative dielectric constant (ε_r) of 3.0 and a loss tangent (tan δ) of 1.3×10^{-3} utilizing a milling machine (LPKF ProtoMat S61 [8]).

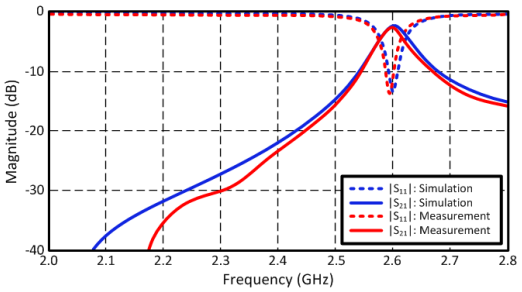

Fig. 3. Simulated and measured scattering parameters (S_{11} & S_{21}) of the tunable filter without fluid sample.

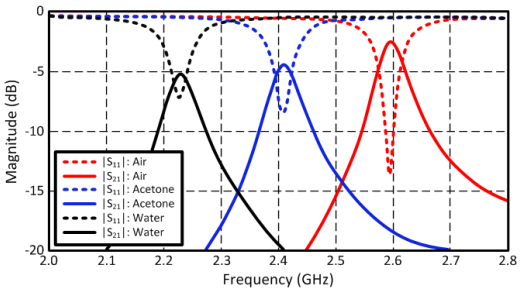

Fig. 4. Measured scattering parameters (S_{11} & S_{21}) of the tunable filter with various fluid samples: acetone and water.

The simulated and measured reflection coefficient (S_{11}) and transmission coefficient (S_{21}) are shown in Fig. 3. The 3D full wave simulator, ANSYS HFSS v11.1, was utilized to design the circuit. The measurements agree with the simulation result very well. The measured center frequency (f_0) of the filter is 2.6 GHz and the 3 dB bandwidth is 54 MHz. The insertion loss (IL) of the filter at the center frequency (f_0) is 2.47 dB. One can note that it can be improved by realizing a smaller gap between the tightly coupled feeding line and the square-ring resonator. Various fluid samples like acetone and water were loaded on the capacitive sensing gap to verify the performance of the designed filter. The complex relative dielectric constants of acetone (99 % purity) and tap water are 19.1 (tan δ = 0.042) [9] and 73.0 (tan δ = 0.11) [10] at room temperature (300 K), respectively.

C. Broadband Antenna Design

A broadband linearly polarized antenna is required to receive and transmit a broadband signal from/to the reader. A microstrip monopole type antenna has been chosen because it features high axial ratio (AR) as well as it is easy to integrate with the designed microstrip square ring resonator filter without any transition. Plus, it has a relatively wide bandwidth compared to resonator-type antennas, such as a patch antenna [11]. A circular disk is used as a load at the end of the monopole antenna to improve the bandwidth [12]. The width of the monopole antenna is 3 mm which is the width of a 50 Ω microstrip line on 1.27 mm (5 mil) thick RO3003 (Fig. 5). The length of the antenna has been chosen to quarter-wavelength ($\lambda_0/4$) of 2.4 GHz, and the diameter (D) of the circular disk and the length (L_2) of the dipole antenna have been optimized to cover the desired operation frequency band (2.2 ~ 2.6 GHz).

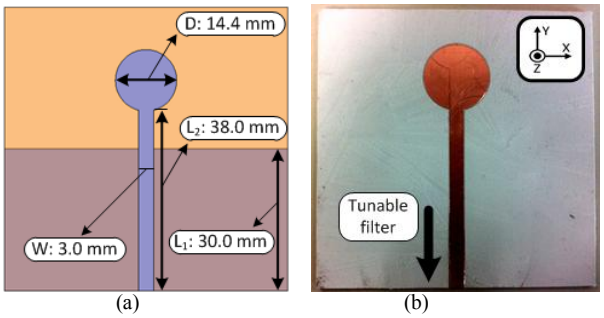

(a) (b)

Fig. 5. (a) Geometry of the proposed microstrip monopole antenna and (b) the fabricated broadband antenna.

The geometry and the fabricated prototype of the disk-loaded microstrip broadband antenna on RO3003 (thickness: 1.27 mm) [7] are shown in Fig. 5. The antenna was fabricated utilizing the same milling machine [8]. The simulated and measured (in an anechoic chamber) reflection coefficient (S_{11}) of the antenna presented in Fig. 6 show good agreement over the investigated frequency range. The small discrepancy results from the fabrication error. The dimensions of the fabricated antenna are slightly smaller by about 200 µm than the designed dimensions due to the slightly larger metal removal during the milling process. The simulation result is obtained for the dimensions shown in Fig. 5. The rough surface and edge which result from the milling process also introduce unwanted parasitic effects [13]. For the simulation, ANSYS HFSS v11.1 has been utilized. The resonant frequency of the antenna is 2.24 GHz and it has a fractional bandwidth of 27.9 % (625 MHz). The simulated radiation patterns on E-plane (YZ-plane) and H-plane (XZ-plane) at 2.24 GHz are shown in Fig. 7. The antenna has an omni-directional radiation pattern over the operation frequency range (2.2 GHz ~ 2.6 GHz). The calculated realized gain values of the antenna at 2.2 GHz, 2.4 GHz, and 2.6 GHz, which are the center frequencies of the loaded tunable filter with the gap filled with water, acetone, and air (no liquid) (Fig. 4) are 2.78 dBi, 3.10 dBi, and 3.18 dBi, respectively. The simulated axial ratio (AR) of the antenna is 66.27 dB at bore-sight. The realized antenna meets every design specification, as it has been experimentally and theoretically verified.

D. Sensor Integration and Sensing Capability

As a proof-of-concept demonstration of the fluid sensing capability, the designed broadband microstrip monopole antenna (Fig. 5) has been integrated with the capacitive gap-loaded tunable filter (Fig. 2). One port (P_1) of the filter was connected to the antenna and the other port (P_2) was connected to a VNA for the reflection coefficient (S_{11}) measurement. Fluid samples (water and acetone) were loaded on the capacitive gap of the tunable filter and the frequency response was measured as shown in Fig. 8. The simulation and measurement of the center frequency variation of the sensor platform (filter and antenna) depending on the sample fluids show very good agreement. The frequency shift of 200 MHz for acetone and 380 MHz for water is a drastically increased frequency shift compared to other reported similar RFID-based sensors [14,15]. To verify the performance of the proposed sensor in terms of repeatability, a series of similar

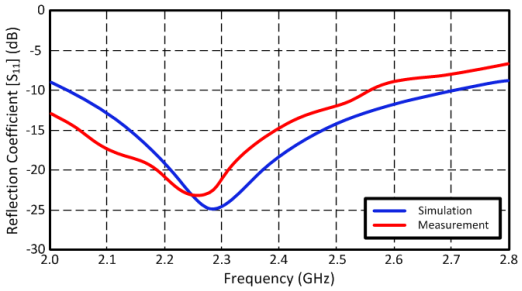

Fig. 6. Simulated and measured reflection coefficient (S_{11}) of the microstrip monopole antenna.

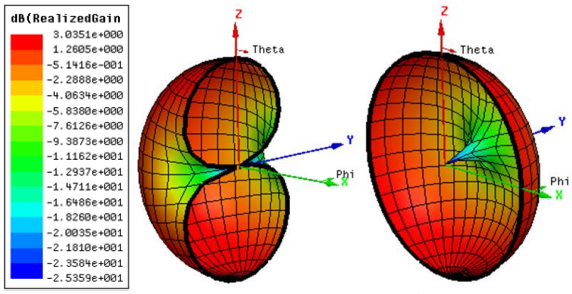

(a) (b)

Fig. 7. Simulated radiation patterns on (a) E-plane (YZ-plane) and (b) H-plane (XZ-plane) at 2.24 GHz.

measurements have been performed. The frequency responses retrieved have demonstrated a very close behavior.

In the final sensor platform, both P_1 and P_2 (Fig. 2(b)) are connected to antennas. The broadband signal from the reader is received by the horizontally polarized antenna, and the broadband signal is filtered by the tunable filter which has a liquid-dependent center frequency. The vertically polarized antenna reradiates the filtered narrowband signal to the reader (Fig. 1). Without a fluid sample, the reflection coefficient value is less than -10 dB at the operation frequency which results in more than 90 % of power to be delivered to the vertically polarized antenna (Fig. 8). The high axial ratio (66.27 dB) of the antennas helps suppress the unwanted re-radiation from the horizontally polarized antenna in the vertical polarization. The interrogation range of the proposed sensor platform can be estimated based on the measured insertion loss of the filter and the calculated antenna gains [18]. The estimated interrogation range is 5.33 m in free space assuming the reader sensitivity is below -60 dBm (sensitivity of commercial RFID reader [16]) with a transmission power of 30 dBm (FCC regulation [17]) from a reader antenna which gain is 6 dBi.

III. INKJET PRINTING OF THE SENSOR PLATFORM

It is important to implement the hereby introduced liquid sensing platform on flexible substrates in order to allow for rugged surface mounting, such as for instance cylindrical pipelines. Subtractive fabrication methods, such as milling and etching, are widely utilized for prototyping due to its ease of feature size control. However, the milling technique is not suitable for thin flexible substrates because its drill bit may damage the substrate. The etching technique can handle a thin flexible material but it utilizes strong acids to wash away the metals and requires masks for patterning. In this case, an additive method like the inkjet printing technology has great potential to implement a low cost environmentally friendly

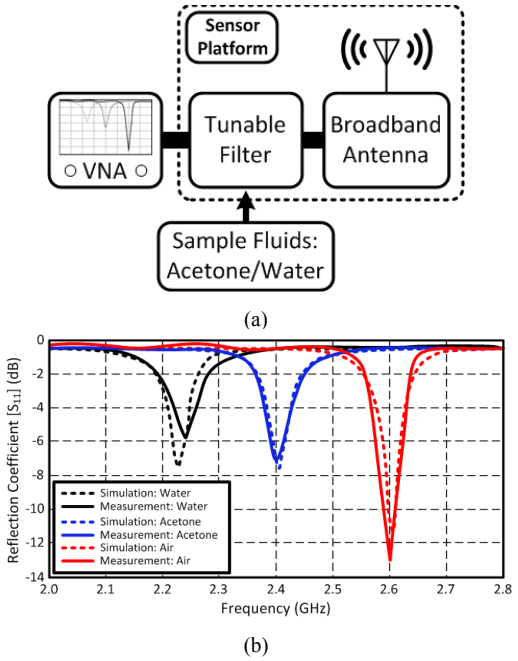

Fig. 8. (a) The measurement setup of the designed sensor platform (the tunable filter and the antenna) and (b) the simulated and measured reflection coefficients (S_{11}) of the chipless sensor platform with different fluids.

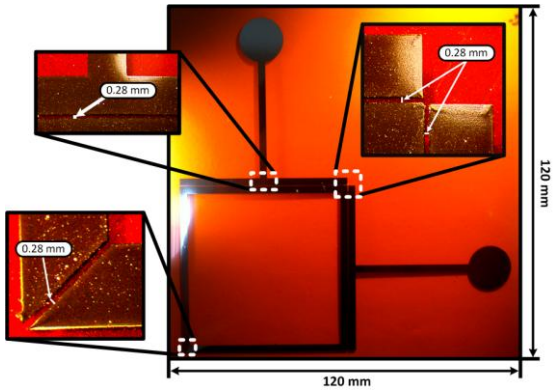

Fig. 9. The inkjet-printed chipless RFID-based fluid sensor platform on a Kapton substrate.

flexible sensor platform because it does not produce any byproducts by just printing the conductive ink on the desired position with an easily controlled amount volume of ink [19]. The inkjet printing of nanoparticle-based ink has been characterized and its capability toward RF applications has been demonstrated in [20-22]. Fig. 9 shows the picture of an inkjet-printed prototype of the proposed sensor platform on Kapton, that demonstrates the realization feasibility of highly scalable low-cost flexible "green" wireless liquid sensors with enhanced sensitivity.

IV. Conclusion

A novel fully passive chipless RFID-based fluidic sensor has been demonstrated. A step-by-step design procedure has been discussed in detail, and the performance of each design component (the capacitive gap-loaded tunable filter and the broadband microstrip monopole antenna) as well as of the whole integrated sensor platform has been experimentally demonstrated. The sensor demonstrates resonant frequency shifts (380 MHz for water and 200 MHz for acetone) drastically greater than those previously reported for similar sensors. The sensor platform has exhibited a high repeatability and could find numerous applications ranging from fluid quality monitoring to pipeline leak and oil exploration. The next step of this work is to implement a complete inkjet-printed flexible low-cost zero-power "green" RFID-based sensor system.

References

[1] H. Liu, M. Bolic, A. Nayak, and I. Stojmenovic, "Taxonomy and Challenges of the Integration of RFID and Wireless Sensor Networks," *IEEE Network*, vol.22, no.6, pp.26–35, 2008.

[2] S. Kim, C. Mariotti, F. Alimenti, P. Mezzanotte, A. Georgiadis, A. Collado, L. Roselli, and M. M. Tentzeris, "No Battery Required: Perpetual RFID-Enabled Wireless Sensors for Cognitive Intelligence Applications," *IEEE Microw. Mag.*, vol.14, no.5, pp.66–77, July 2013.

[3] R. Want, "Enabling Ubiquitous Sensing with RFID," *Computer*, vol.37, no.4, pp.84–86, Apr. 2004.

[4] V. K. Tripathi and I. Wolff, "Perturbation Analysis and Design Equations for Open- and Closed-Ring Microstrip Resonators," *IEEE Trans. Microw. Theory Techn.*, vol.32, no.4, pp.405–410, Apr. 1984.

[5] L. Zhu and K. Wu, "A Joint Field/Circuit Model of Line-to-Ring Coupling Structures and Its Application to the Design of Microstrip Dual-Mode Filters and Ring Resonator Circuits," *IEEE Trans. Microw. Theory Techn.*, vol.47, no.10, pp.1938–1948, Oct. 1999.

[6] S. Luo, L. Zhu, and Sheng Sun, "A Dual-Band Ring-Resonator Bandpass Filter Based on Two Pairs of Degenerate Modes," *IEEE Trans. Microw. Theory Techn.*, vol.58, no.12, pp.3427–3432, Dec. 2010.

[7] [Online] http://www.rogerscorp.com/documents/722/index.aspx

[8] [Online] http://www.lpkfusa.com/RapidPCB/CircuitboardPlotters/s62.htm

[9] P. Lidström, J. Tierney, B. Wathey, and J. Westman, "Microwave Assisted Organic Synthesis – A Review," *Tetrahedron*, vol.57, no.45, pp.9225–9283, Nov. 2001.

[10] K. Shibata, "Measurement of Complex Permittivity for Liquid Materials Using the Open-ended Cut-off Waveguide Reflection Method," in *Proc. 2011 Microwave Conference Proceedings (CJMW)*, Hangzhou, China, pp.1–4, Apr. 2011.

[11] Z. N. Chen, M. J. Ammann, X. Qing, X. H. Wu, T. S. P. See, and A. Cat, "Planar Antennas," *IEEE Microw. Mag.*, vol.7, no.6, pp.63–73, Dec. 2006.

[12] W. -C. Liu, C. -M. Wu, and Y. -J. Tseng, "Parasitically Loaded CPW-Fed Monopole Antenna for Broadband Operation," *IEEE Trans. Antennas Propag.*, vol.59, no.6, pp.2415–2419, June 2011.

[13] I. Minis, R. Yanushevsky, A. Tembo, and R. Hocken, "Analysis of Linear and Nonlinear Chatter in Milling," *CIRP Ann. Manuf. Technol.*, vol.39, no.1, pp.459–462, Jan. 1990.

[14] B. Cook, J. Cooper, S. Kim, and M. M. Tentzeris, "A Novel Inkjet-Printed Passive Microfluidic RFID-based Sensing Platform," *IEEE MTT-S International Microwave Symposium Digest (MTT)*, Seattle, WA, 2013.

[15] R. S. Nair, E. Perret, S. Tedjini, and T. Baron, "A Group-Delay-Based Chipless RFID Humidity Tag Sensor Using Silicon Nanowires," *IEEE Antennas Wireless Propag. Lett.*, vol 12, pp.729–732, June 2013.

[16] [Online] http://www.impinj.com/Applications/White_Papers.aspx.

[17] Understanding the FCC regulations for low-power, non-licensed transmitters, Federal Communications Commission (FCC), OET Bulletin no.63, Feb. 1996.

[18] K. V. S. Rao, P. V. Nikitin, and S. F. Lam, "Antenna design for UHF RFID tags: a review and a practical application," *IEEE Trans. Ant. Prop.*, vol.53, no.12, pp.3870–3876, Dec. 2005.

[19] J. Perelaer, A. W. M. de Laat, C. E. Hendriks, and U. S. Schubert, "Inkjet-printed Silver Tracks: Low Temperature Curing and Thermal Stability Investigation," *J. Mater. Chem.*, vol.18, no.27, pp.3209–3215, June 2008.

[20] L. Yang, A. Rida, R. Vyas, and M. M. Tentzeris, "RFID Tag and RF Structures on a Paper Substrate Using Inkjet-Printing Technology," *IEEE Trans. Microw. Theory Techn.*, vol.55, no.12, pp.2894–2901, Dec 2007.

[21] V. Pynttäri, E. Halonen, H. Sillanpää, M. Mäntysalo, and R. Mäkinen, "RF Design for Inkjet Technology: Antenna Geometries and Layer Thickness Optimization," *IEEE Antennas Wireless Propag. Lett.*, vol.11, pp.188–191, Mar. 2012.

[22] S. Kim, A. Georgiadis, A. Collado, and M. M. Tentzeris, "A Inkjet-Printed Solar-Powered Wireless Beacon on Paper for Identification and Wireless Power Transmission Applications," *IEEE Trans. Microw. Theory Techn.*, vol.60, no.12, pp.4178–4186, Dec. 2012.